HHS Public Access

Author manuscript

Cancer. Author manuscript; available in PMC 2020 November 01.

Published in final edited form as:

Cancer. 2019 November 01; 125(21): 3738–3748. doi:10.1002/cncr.32366.

Tumor characteristics associated with engraftment of patient-derived non-small cell lung cancer xenografts in immunocompromised mice

Yungchang Chen[1,2], **Ran Zhang**[1], **Li Wang**[1], **Arlene M. Correa, PhD**[1], **Apar Pataer, MD, PhD**[1], **Yi Xu, PhD**[1], **Xiaoshan Zhang, PhD**[1], **Chenghui Ren**[1], **Shuhong Wu**[1], **Qing H Meng, PhD**[3], **Junya Fujimoto, MD**[4], **Vanessa B. Jensen, DVM**[5], **Mara B. Antonoff, MD**[1], **Wayne L. Hofstetter, MD**[1], **Reza J. Mehran, MD**[1], **George Pisimisis, MD**[1], **David C. Rice, MD**[1], **Boris Sepesi, MD**[1], **Ara A. Vaporciyan, MD**[1], **Garrett L. Walsh, MD**[1], **Stephen G. Swisher, MD**[1], **Jack A. Roth, MD**[1], **John V. Heymach, MD, PhD**[6], **Bingliang Fang, MD**[1,*]

[1]Department of Thoracic and Cardiovascular Surgery, The University of Texas MD Anderson Cancer Center, Houston, Texas, USA.

[2]Department of Medical Oncology, Sun Yat-Sen University Cancer Center and Collaborative Innovation Center of Cancer Medicine of The First People's Hospital of Foshan, Guangdong, China.

[3]Department of Laboratory Medicine, The University of Texas MD Anderson Cancer Center, Houston, Texas, USA.

[4]Department of Translational Molecular Pathology, The University of Texas MD Anderson Cancer Center, Houston, Texas, USA.

[5]Department of Veterinary Medicine and Surgery, The University of Texas MD Anderson Cancer Center, Houston, Texas, USA.

[6]Department of Thoracic/Head and Neck Medical Oncology, The University of Texas MD Anderson Cancer Center, Houston, Texas, USA.

[*]**Corresponding author:** Bingliang Fang, Department of Thoracic and Cardiovascular Surgery, The University of Texas MD Anderson Cancer Center, 1515 Holcombe Blvd., Unit 1489, Houston, TX 77030, USA; phone: (713) 563-9147; fax: (713) 794-4901; bfang@mdanderson.org.

AUTHOR CONTRIBUTIONS

Bingliang Fang: designed and directed the study and wrote the first draft of the manuscript. **Yungchang Chen**: performed data analysis and participated in writing of the manuscript. **Ran Zhang, Li Wang, Arlene M. Correa, Apar Pataer MD, Yi Xu, Xiaoshan Zhang PhD[1], Chenghui Ren, Shuhong Wu, Qing H, Meng, Junya Fujimoto, Vanessa B. Jensen**: performed data analysis and interpretations. **Mara B. Antonoff, Wayne L. Hofstetter, Reza J. Mehran, George Pisimisis, David C. Rice, Boris Sepesi, Ara A. Vaporciyan, Garrett L. Walsh, Stephen G. Swisher, Jack A. Roth, John V. Heymach**: contributed in clinical specimen and data collections.

AVAILABILITY OF DATA AND MATERIALS

All data generated or analyzed during this study are included in this manuscript and its supplemental file.

CONSENT FOR PUBLICATION

Not applicable

ETHICS APPROVAL AND CONSENT TO PARTICIPATE

Fresh lung cancer samples were collected from surgically resected specimens under research protocols approved by the Institutional Review Board at The University of Texas MD Anderson Cancer Center. All clinical samples and data were collected with informed consent from the patients.

CONFLICTS OF INTEREST

The authors declare that they have no competing interests.

Abstract

Background: Patient-derived xenograft (PDX) models are increasingly used in translational research, however, the engraftment rates of patient tumor samples in immunodeficient mice to PDX models vary greatly.

Methods: Tumor tissue samples from 308 NSCLC patients were implanted in immunodeficient mice. The patients were followed for 1.5 to about 6 years. We performed histological analysis of PDXs and some residual tumor tissues in mice with failed PDX growth at 1 year after implantation. Quantitative PCR and ELISA were performed to measure the levels of Epstein-Barr virus genes and human immunoglobulin G in PDX samples. Patients' characteristics were compared for PDX growth and overall survival as outcomes using cox regression analyses.

Results: Overall engraftment rate of NSCLC PDXs was 34%. Squamous cell carcinomas had a higher engraftment rate (53%) than did adenocarcinomas. Tumor samples from patients with stage II and III diseases and from larger tumors had relatively high engraftment rates. Patients whose tumors successfully engrafted had worse overall survival, particularly those with adenocarcinoma, stage III or IV disease, and moderately differentiated tumors. Lymphoma formation was one of factors associated with engraftment failures. Human CD8+ and CD20+ cells were detected in residual samples of tumor tissue that failed to generate a PDX at 1 year after implantation. Human immunoglobulin G was detected in the plasma of mice that did not have PDX growth at 14 months after implantation.

Conclusions: Our results indicate that characteristics of cancer cells and tumor immune microenvironment in primary tumors can both affect engraftment of a primary tumor sample.

Precis:

This study identified clinical tumor characteristics, biological features of cancer cells, and tumor immune microenvironment are associated with successful engraftment of tumor samples. Patients' immune cells can be present for a long time in residual tissue from failed PDXs, which indicates that these immune cells may play roles in inhibiting PDX engraftment.

Keywords

Tumor models; xenografts; neoplasia; NSCLC; tumor microenvironment

Introduction

Patient-derived xenograft (PDX) mouse models are used preclinically in cancer drug development and molecular profiling of tumors. They have been shown to recapitulate the histologic and genetic features of human primary tumors and to be useful in assessing treatment response. Evidence has shown that PDXs retain the genome-wide exomic nucleotide variants, gene copy-number alterations, and DNA methylation patterns of their corresponding tumors [1–4] irrespective of the number of passages [1, 3], although clonal selection during initial engraftment and passaging of PDXs has been observed [5, 6]. In vivo propagation of a patient's tumor tissue in immunodeficient mice can enable simultaneous evaluation of the tumor response to several drugs and treatment regimens, leading to the identification of an effective therapy for the patient [7, 8]. An analysis of the treatment

responses of PDXs established from 92 patients with different solid tumors revealed a significant association between drug response in patients and the response in mice bearing the corresponding PDXs, indicating that PDXs can predict clinical treatment response [4]. PDX models are also increasingly employed in the mechanistic characterization of resistance to targeted therapies [9–11], the identification of novel biomarkers [12] and therapeutic targets [13], and the characterization of intratumoral heterogeneity [14, 15].

Molecular characterization of lung cancer PDXs has revealed that these PDXs faithfully retain genomic alterations found in their corresponding primary tumors [2, 16]. Lung tumor PDXs also recapitulate clinically observed tumor response to chemotherapy and targeted therapy. For example, the response rate to paclitaxel treatment in PDXs was equivalent to that reported in a clinical study of paclitaxel single-agent therapy for patients with advanced non-small cell lung cancer (NSCLC) [17], and PDXs harboring targetable driver mutations (*EGFR, ALK, ROS1)* had similar response patterns to target inhibitors as did patient tumors [18–20]. Although several groups have devoted effort to generating and characterizing NSCLC PDXs, the overall PDX engraftment rates for NSCLC range from 25% to 40% [2, 20–22], lower than the engraftment rates reported for colorectal cancer [23] and melanoma PDXs [24].

We previously reported an overall engraftment rate of 26% for NSCLC specimens in nonobese diabetic/severe combined immunodeficiency (NOD SCID) mice [16]. The engraftment rate rose to about 35% when NOD SCID mice with null mutations of the gene encoding for the interleukin-2 receptor-γ (NSG mice) were used for PDX generation. Over the past 6 years, we have generated 105 NSCLC PDXs using tissue samples from 308 patients. Some of these PDX models have been used for preclinical evaluation of anticancer agents [25–27] and are available to the cancer research community through the National Cancer Institute's PDXNet program (www.pdxfinder.org). To better understand what drives the relatively low engraftment rates of NSCLC PDXs and to identify factors that could improve engraftment rates, we analyzed clinical parameters that were associated with the engraftment rate of PDXs from 308 NSCLC patients who were followed up for 1.5 to about 6 years after sample acquisition. Our results showed that the PDX engraftment rate was significantly higher for squamous cell carcinomas than for other NSCLC. The PDX engraftment rate was higher for tumor samples from patients with stage II and III disease or relatively large tumors. Patients whose tumors formed PDXs had significantly shorter overall survival durations than did patients whose tumors did not form xenografts, particularly for patients with non-squamous cell carcinoma, moderate histologic differentiation, or stage II or IV disease. Interestingly, tissue residuals from tumor samples that did not form PDXs contained human CD8+ and CD20+ immune cells, suggesting tumor immune microenvironment may play a role in PDX engraftment.

Materials and Methods

Primary tumor samples and clinical data

Fresh NSCLC tumor samples were collected from 2012 to 2017 from surgically resected specimens. A few pleural fluid drainage samples and biopsy samples were also collected for establishing PDXs. The clinical data, including pathological diagnosis and survival data, were collected from patient records. The protocols for the use of clinical specimens and data

in this study were approved by the Institutional Review Board at The University of Texas MD Anderson Cancer Center. All clinical samples and data were collected with the informed consent of the patients.

Generation of PDXs

PDXs were established from surgically resected specimens or from pleural fluid as we previously reported [16, 28]. We used NOD SCID mice for generating PDXs during 2012 and 2013. Since 2014, we have used NSG mice for generation and passaging of PDXs. Both NOD SCID and NSG mice were obtained from Jackson Laboratory (Bar Harbor, ME) or from our institutional Research Animal Support Facility. All animal studies were carried out in accordance with the Guidelines for the Care and Use of Laboratory Animals (National Institutes of Health Publication 85–23) and the institutional guidelines of MD Anderson Cancer Center. Animals were maintained at our institutional Research Animal Support Facility.

For generating PDXs from surgical and biopsy samples, freshly harvested tumor tissue was placed in serum-free RPMI medium supplemented with 100 μg/mL penicillin-streptomycin (both from Invitrogen, Carlsbad, CA) and implanted into the rear flank subcutaneous space of mice within 2 hours of surgical resection, as we previously described [16]. For generating PDXs from pleural fluid, the fluid samples were centrifuged to collect cell pellets. Red blood cells in the samples were lysed with sterile buffer (150 mM NH_4Cl, 20 mM Tris-Cl, pH 7.4), and the pellets were washed twice with PBS. About 2×10^7 cells were inoculated into the rear flank subcutaneous area of NSG mice. The mice were monitored for up to 15 months for tumor growth and were euthanized if no sign of tumor growth. The tumors were harvested when they reached 1.5 cm in diameter. The harvested tumors (labeled F1 for the first passage in animals) were chopped into 2-to-3-mm^3 pieces, which were frozen in liquid nitrogen for future investigation and/or molecular characterization, fixed in formalin and embedded in paraffin for histological analysis, or reimplanted into nude mice or NSG mice to generate more tumor grafts (F2, F3, etc., for subsequent passages).

Histological analysis of PDXs

Histological analysis of PDXs and their primary tumor tissues was performed using hematoxylin and eosin staining of paraffin-fixed tissue sections. Immunohistochemical staining of formalin-fixed paraffin-embedded tumor tissue on slides was performed at the Research Histology, Pathology and Imaging Core Facility at MD Anderson. Slides bearing tumor tissue sections were stained with mouse monoclonal antibodies specific for human wide-spectrum cytokeratin (Abcam, Cambridge, UK; ab9377), CD8 (eBioscience, San Diego, CA; clone C8/144B), and CD20 (Bio-Rad, Hercules, CA; MCA2454) using the standard operating protocols used by the Core Facility. Mouse immunoglobulin G (IgG) was used as a negative control. Human lymph node samples were used as positive controls for the anti-human CD8 and CD20 antibodies.

DNA fingerprinting and quantitative PCR analysis

DNA was isolated from primary tumor samples and PDX tissues by proteinase K digestion (20 mg/mL), phenol extraction, and isopropanol precipitation. DNA samples were dissolved

in water and quantified with a Quant-iT PicoGreen dsDNA Assay Kit (Thermo Fisher) following the manufacturer's instructions. DNA fingerprint assays were performed to verify the provenance of DNA from primary tumors and PDXs. This assay was performed at our institution's Characterized Cell Line Core Facility using the PowerPlex 16 HS System (Promega). The short tandem repeat profiles were compared with those of case-matched specimens obtained from the patients and/or with 2455 known profiles in online databases (American Type Culture Collection [ATCC], German Collection of Microorganisms and Cell Culture [DSMZ], Japanese Collection of Research Bioresources [JCRB], and RIKEN Cell Bank) and 2556 known profiles in the MD Anderson Characterized Cell Line Core database.

Quantitative PCR (qPCR) using Sybr Green PCR Master Mix (Thermo Fisher) was used to determine the presence of Epstein-Barr virus (EBV) DNA in PDXs and primary tumor samples. The human *PERK* gene was used as the reference. The sequences of the primers used for detecting the EBV *EBNA1* gene and the human *PERK* gene were EBNA1-F: 5′-CGTCTCCCCTTTGGAATGG-3′; EBNA1-R: 5′-GAAATAACAGACAATGGACTCCCTTAG-3′; PERK-F: 5′-CTGTTCAGCTCTGGGTTGTC-3′; and PERK-R: 5′-TGGGTACGCTGTAGAAGCAG-3′. Eight nanograms of genomic DNA was added to the qPCR Master Mix (Thermo Fisher, 4371355) at a final reaction volume of 10 μL and 100 nM of each primer. The PCR conditions were 95°C for 10 min followed by 40 cycles of 95°C for 15 s and 60°C for 1 min. Melting curves were generated after amplification. Relative copy numbers were evaluated using the relative standard curve method and normalized to the *PERK* gene levels. qPCR was carried out using a CFX384 Real-Time System (Bio-Rad) at 50°C for 2 minutes, 95°C for 10 minutes, 92°C for 15 seconds, 62°C for 1 minute + plate read for a total of 40 cycles. Each sample was analyzed in duplicate, and copy number of *EBNA1* were normalized to that of human *PERK* gene.

ELISA

The levels of human IgG in mouse plasma were measured using ELISA kit (Human IgG ELISA kit, Invitrogen Thermo Fisher Scientific, Carlsbad, CA) following the manufacturers' instructions. Briefly, blood samples were collected in BD Microtainer tubes containing EDTA. Plasma samples were stored at −80°C until use. After thawing, plasma was diluted to a ratio of approximately 1:10 to 1:30 with dilution buffer, and 100 μL of diluted samples and serially diluted IgG standards were added in duplicate to the wells of a 96-well plate precoated with capture antibodies. After incubating at room temperature for 2 hours, the plates were washed with PBS containing 0.05% Tween 20 and incubated with biotinylated detection antibodies and horseradish peroxidase-conjugated streptavidin. The enzymatic activity of horseradish peroxidase was determined with its substrate 3,3′,5,5′-tetramethylbenzidine by measuring absorbance at 450 nm using a 96-well-plate reader (FLUOstar Omega, BMG Labtech GmbH, Offenburg, Germany). IgG concentrations were calculated from the standard curve.

Statistical analysis

Two-tailed Student *t* tests or Fisher exact tests were used to compare the tested parameters in different groups. Differences were considered statistically significant at $P < 0.05$. Associations between categorical variables were analyzed with the Pearson chi-square or Fisher exact tests. For continuous variables, we used the Mann-Whitney *U* test. Univariate Cox regression analysis was performed using death as the outcome with a significance level of $P < 0.05$. Covariates that were significant at $P < 0.25$ were included in a multivariable Cox regression. Backward stepwise Wald elimination at $P = 0.10$ was used to establish the final model. Patients with incomplete data were excluded from the multivariable analysis. Survival functions were calculated according to the Kaplan-Meier method, and differences were assessed with the log-rank test. Univariate and multivariable logistic regression analyses using PDX growth as the outcome were performed using the same strategy described for the multivariable Cox regression analysis. All statistical analyses were performed using SPSS software version 24.0 (SPSS Inc., Chicago, IL).

RESULTS

Patient and tumor characteristics associated with successful PDX growth

We collected fresh surgically resected tumor samples from 308 patients who had been diagnosed with NSCLC during 2012 to 2017 and implanted them in immunodeficient mice to generate PDXs. PDXs were successfully generated from 105 tumor implants and were passaged for 2 to 6 generations. The time from implantation of the fresh surgical specimen to harvest (when the palpable mass reached 1.5 cm in diameter) ranged from 1 to 12 months, with a mean time to harvest of 4.5 months. The overall engraftment rate was 34%. In NOD SCID mice, which we used to generate PDXs during 2012 and 2013, the overall engraftment rate was about 26%. After 2013, we used NSG mice for generation of PDXs, which increased engraftment rates to 35%. Eighty percent of the PDXs generated in NSG mice were successfully passaged in nude mice. The remaining 20% of the PDXs generated in NSG mice did not grow in nude mice, but readily grew in NSG mice. We also successfully generated 7 PDXs from 18 pleural fluid samples and biopsy samples in NSG mice. Since most of our samples were from surgically resected tumors, we analyzed clinical characteristics that may affect engraftment rates of surgically resected specimens.

The demographic and clinical characteristics of the 308 lung cancer patients whose tumor specimens were implanted for generation of lung tumor PDXs are shown in Supplemental Table 1. Univariate logistic regression analysis showed that several factors were significantly associated with engraftment rate ($P < 0.05$). Squamous cell carcinomas had a higher engraftment rate (53.4%) than did adenocarcinoma (29.0%) or other histological types (31.6%). Poorly differentiated tumors had a higher engraftment rate (49.3%) than did well-differentiated (19.3%) or moderately differentiated tumors (32.3%). Larger tumors and tumors from patients with stages II or III disease had higher engraftment rates (45% ~ 51%) than did smaller tumors (26%) and tumors from patients with stage I disease (22%) (Figure 1). In contrast, preoperative chemotherapy had no significant effect on tumor engraftment rates. Multivariable logistic regression analysis showed that tumor histology and stage had

significant effects on engraftment rates, whereas the effect of tumor size did not reach statistical significance ($P = 0.096$).

Lymphoma formation is one of the factors leading to failed PDX growth

Proliferation of EBV-positive B cells present in NSCLC tumor samples implanted in immunocompromised mice has been reported to lead to the formation of human diffuse large B-cell lymphoma and loss of the carcinoma component of xenograft tumors [29]. Formation of human B-cell lymphoma in NSG mice during PDX generation has also been reported for other types of cancer, including melanoma [30], gastrointestinal cancer [31], and breast, colon, pancreatic, bladder and renal cancer [32]. We observed lymphoma formation in 17 cases whose xenograft tumors consisted predominantly of human B lymphocytes. These cases were grouped as no PDX growth. The lymphomas usually formed at the subcutaneous sites of tumor implantation, but we also observed metastases in the lymph nodes, spleen, and liver. Tumors harvested from mice with lymphomas predominantly consisted of human CD19+ or CD20+ B cells, with only scattered small islands of pan-cytokeratin-positive epithelial cells (Figure 2A). Lymphoma formation was observed in mice implanted with adenocarcinoma, squamous cell carcinoma, and carcinoid tumor samples. Moreover, we found that lymphoma formation could occur during passaging of PDXs; that is, the tumor tissues harvested from the second passage of an established PDX could be NSCLC in one mouse and lymphoma in another mouse (Figure 2). This finding strongly indicates that researchers should be cautious about possible pathological alterations during passaging of PDX models during preclinical studies.

We performed PCR to determine the levels of the EBV gene *EBNA1* in DNA isolated from PDXs, lymphomas, and their associated primary NSCLC tumors, using the human *PERK* gene as a control. DNA samples from white blood cells of healthy donors were used as normal controls. The analysis showed that the *EBNA1* copy number were significantly higher lymphoma than all other groups ($P < 0.01$) (Figure 2B). There was no significant difference in the number of *EBNA1* copies among the samples of normal controls, PDXs, and primary NSCLC tumors that lead to PDX or lymphoma formation, although a few outliers with relatively high *EBNA1* copy numbers were detected in primary NSCLC tumor samples that produced lymphoma or PDXs (Figure 2B). This result suggested that the majority of the observed lymphoma were positive for EBV. However, levels of *EBNA1* DNA in primary tumors may not accurately predict lymphoma formation after implantation.

Patients' lymphocytes in residual tumor tissues of failed PDX growth

Our recent study showed that patient-derived tumor immune cells, including T cells (CD8+ or CD4+), B cells (CD19+) and macrophages (CD68+), were detected in approximately 36% of early passage lung cancer PDXs [28]. Human tumor-infiltrating immune cells that are coimplanted along with tumor tissues might have anticancer activity that leads to failure of PDX growth. To test whether human immune cells were present in residual tumor tissue that failed to generate PDX growth, we harvested residual tumor tissues from sites of tumor implantation in 5 mice that had no sign of PDX growth at 12 months or more after tumor implantation. Histopathological analysis revealed that 4 of the 5 residual tissue specimens mainly consisted of scar-like fibrotic tissue, with scattered or clustered inflammatory cells

and a few viable epithelial cells; the remaining one mainly consisted of viable tumor cells surrounded by stromal tissue. Immunohistochemical staining revealed that the inflammatory cells in the 4 specimens with scar-like tissue were mainly human CD8+ and/or CD20+ cells (Figure 3). However, no CD8+ or CD20+ cells were detected in the 5th specimen, which had predominantly pan-cytokine-positive epithelial cells. The long-term (> 12 month) survival of tumor-infiltrating lymphocytes in residual tumor tissues indicated that they might play a role in preventing PDX growth. However, in some cases, such as the one we observed, in which failure of PDX growth cannot be attributed to coimplantation of tumor-infiltrating lymphocytes.

To test whether the human lymphocytes detected in the residual tumor tissues were still functional, we performed ELISA for human IgG in plasma samples from 13 mice that did not exhibit PDX growth at 14 months after implantation of 6 human primary tumor samples. Plasma from naïve NSG mice that had not undergone implantation of human samples was used as controls. All of the mice that had received human tumor implants had human IgG in their plasma, although the concentration ranged widely, from 0.73 μg/mL to 8.07 μg/mL (Figure 4). In contrast, the control mice had only background levels of human IgG (< 0.5 μg/mL). This result demonstrated that human B cells coimplanted with tumor tissues were functional at 14 months after implantation.

PDX growth and clinical outcomes

We performed univariate and multivariable Cox regression analyses to determine whether PDX growth or lymphoma formation from surgically resected tumors was associated with clinical outcomes. The 308 patients included in this analysis had a median follow-up time of 3 years (range: 1.5 – 6 years). For the 290 patients with stage I-III NSCLC, we determined whether recurrence and/or metastasis developed after surgical resection of the tumor. Among these patients, 84 developed advanced disease including both recurrence and metastasis: 46 in 190 cases (24.2%) whose tumors did not produce PDXs and 38 in 100 cases (38.0%) whose tumors did produce PDXs. The difference between these 2 groups was significant ($P = 0.0202$). Univariable analysis also showed that patients whose tumors produced PDXs had shorter overall survival (OS) durations than did patients whose tumors did not generate PDXs (HR: 2.56, 95% CI: 1.53–4.27, $P < 0.001$). In contrast, we found no differences in OS between patients whose implanted tumors formed lymphomas in mice and other patients. Multivariable analysis showed that shorter OS was significantly associate with advanced disease stage and poor differentiation, and PDX growth increased the risk of death in patients with these characteristics, though not significantly so (HR: 1.69, 95% CI: 0.97–2.97, $P = 0.066$) (Supplemental Table 2).

We also adjusted the OS analysis for tumor type, stage, and grade. The results showed that PDX growth was significantly associated with shorter OS in patients with adenocarcinoma ($P = 0.005$) and other histological types ($P = 0.013$), but not in patients with squamous cell carcinoma ($P = 0.459$). PDX growth was also significantly associated with short OS in patients with stage III or stage IV disease ($P \leq 0.001$) and in patients with moderately differentiated tumors ($P = 0.008$), but not in patients with early-stage disease or those with poorly differentiated or well-differentiated tumors (Figure 5). This result indicated that PDX

growth could be a predictor for poor prognosis for certain subsets of NSCLC patients, including patients with adenocarcinoma, those with advanced disease, and those with moderately differentiated tumors.

Discussion

We found that the success of PDX engraftment can be affected by both the histological subtype of cancer cells and the immune microenvironment of fresh tumor tissues. Our analysis of PDX engraftment from surgically resected tumor specimens from 308 NSCLC patients found an overall engraftment rate of about 35% in NSG mice. Specimens from squamous cell carcinomas, stages II and III tumors, and poorly differentiated tumors had higher engraftment rates than did specimens from adenocarcinomas, stage I tumors, and well-differentiated tumors. In addition, some subsets of patients whose tumors successfully engrafted in mice had a higher rate of disease recurrence and worse OS. This finding was, in general, consistent with reports by others on the association of PDX engraftment of NSCLC tumors and poor OS [2, 33]. We also found that residual tumor tissue obtained from mice in which PDXs had not formed at 12 or more months after implantation of primary tumors often contained human CD8+ and/or CD20+ immune cells, indicating that the coimplantation of tumor-infiltrating immune cells with fresh tumor samples might be one of the factors preventing PDX growth in immunodeficient mice.

Several factors contribute to the success or failure of PDX engraftment. Technical skill of tumor sample inoculation could be one of factors contributing to engraftment rate. In this study, initial sample inoculations were performed mainly by two laboratory staff. We did not notice dramatic difference in their technical skills. The number of viable cancer cells present in the tissue fragments implanted in the mice can be a major factor affecting the engraftment rate. Unfortunately, this information is not available for the samples used in this study. The source of the specimen may also be important; in one study, specimens from NSCLC brain metastases had a significantly higher engraftment rate than did primary NSCLC tumors (74% vs. 23%) [22]. In addition, the conditions to which the tumor specimens are exposed before implantation can affect the success of engraftment; prolonged (> 2 hours) exposure to warm temperatures and prolonged (> 10 hours) ex vivo ischemia were associated with lower engraftment rates [34]. Moreover, as shown in the present study and reported by others, the intrinsic characteristics of primary tumors, such as histology and degree of differentiation, could be a major factor affecting the engraftment rate [2, 33]. The proliferation of EBV-positive B cells in tumor samples has also been reported to cause the formation of human B-cell lymphomas and the failure of PDX growth in specimens from patients with several types of cancer, including lung cancer [29, 31, 32]. A single dose of the anti-CD20 antibody rituximab during the primary tumor implantation process was reported to reduce the frequency of lymphoma formation and rescue PDX growth in a study of ovarian cancer PDXs [35]. In addition to lymphoma, immune cells present within tumor samples and cotransplanted into the subcutis of NSG mice can induce graft-versus-host disease before successful primary tumor engraftment [30], or co-exist with tumor cells in early passages of PDXs [28]. We observed lymphoma formation in over 15% of tumors harvested after implantation of primary tumors and/or during early passages of established PDXs. Thus, one should be alert on possible pathological alterations during passaging of PDX models during the studies.

However, lymphoma formation was not significantly associated with EBV gene copy number in the primary tumor or with patient prognosis.

Two intriguing findings of our study were that human lymphocytes remained in engrafted tumor residual tissues for up to 12 months and that human IgG was detected in the plasma of NSG mice at 14 months after tumor implantation. Early studies showed that ex vivo-expanded tumor-infiltrating lymphocytes infused back to patients [36] or mice [37] were detectable in peripheral blood for about 100 to 120 days. Another early study showed that implantation of fresh human lung cancer tissues into the subcutis of SCID mice resulted in a sustained tumor histologic architecture with a tumor-infiltrating lymphocyte interface and the presence of human IgG in mouse plasma for up to 22 weeks [38]. More recently, it was reported that intratumoral sustained release of recombinant human interleukin-12 in human lung tumor tissue implanted into NSG mice resulted in a prolonged presence of effector memory T cells and CD138+ plasma cells within the tumor xenograft (for up to 9 weeks) [39]. Our results showed that co-implanted human immune cells can survive for much longer in the tumor tissues/residuals in NSG mice than previously known. Moreover, the detection of CD8+ T cells and CD20+ B cells in the residual tumor tissue suggested that these cells may play roles in suppressing PDX growth in NSG mice. The antitumor activity of tumor-infiltrating CD8 T cells is well documented. The role of tumor-infiltrating B cells is less clear [40], although signatures with high levels of tumor-infiltrating B cells or plasma cells were associated with better clinical outcomes for NSCLC patients [41, 42]. Nevertheless, because only tiny residual tumor samples were available at 12 months after implantation, the functionality and clonal diversity of the immune cells present in the residual tissues could not be characterized in this study. Thus, it is not yet clear whether these immune cells are causes of the failure of PDX growth. The fact that one of the residual tumor tissue samples had surviving tumor cells but no detectable immune cells suggests that other factors also contribute to the failure of PDX growth.

Supplementary Material

Refer to Web version on PubMed Central for supplementary material.

ACKNOWLEDGMENT

We thank Amy Ninetto and the Department of Scientific Publications at The University of Texas MD Anderson Cancer Center for editorial review of the manuscript.

FUNDING SUPPORT

This work was supported in part by the National Institutes of Health through grant R01CA190628, The University of Texas PDX Development and Trial Center grant U54CA224065, Specialized Program of Research Excellence (SPORE) grant CA070907, and The University of Texas MD Anderson Cancer Center support grant P30CA016672 (used the Characterized Cell Line Core Facility and Research Animal Support Facility); and by funds from the University Cancer Foundation via the Lung Cancer Moon Shot Program and the Sister Institution Network Fund at The University of Texas MD Anderson Cancer Center.

References

1. Sivanand S, Pena-Llopis S, Zhao H, et al. A validated tumorgraft model reveals activity of dovitinib against renal cell carcinoma. Sci Transl Med. 2012;4: 137ra175.

2. Wang D, Pham NA, Tong J, et al. Molecular heterogeneity of non-small cell lung carcinoma patient-derived xenografts closely reflect their primary tumors. Int J Cancer. 2017;140: 662–673. [PubMed: 27750381]

3. Gao H, Korn JM, Ferretti S, et al. High-throughput screening using patient-derived tumor xenografts to predict clinical trial drug response. Nat Med. 2015;21: 1318–1325. [PubMed: 26479923]

4. Izumchenko E, Paz K, Ciznadija D, et al. Patient-derived xenografts effectively capture responses to oncology therapy in a heterogeneous cohort of patients with solid tumors. Ann Oncol. 2017;28: 2595–2605. [PubMed: 28945830]

5. Eirew P, Steif A, Khattra J, et al. Dynamics of genomic clones in breast cancer patient xenografts at single-cell resolution. Nature. 2015;518: 422–426. [PubMed: 25470049]

6. Ben-David U, Ha G, Tseng YY, et al. Patient-derived xenografts undergo mouse-specific tumor evolution. Nat Genet. 2017;49: 1567–1575. [PubMed: 28991255]

7. Hidalgo M, Bruckheimer E, Rajeshkumar NV, et al. A pilot clinical study of treatment guided by personalized tumorgrafts in patients with advanced cancer. Mol Cancer Ther. 2011;10: 1311–1316. [PubMed: 21673092]

8. Morelli MP, Calvo E, Ordonez E, et al. Prioritizing phase I treatment options through preclinical testing on personalized tumorgraft. J Clin Oncol. 2012;30: e45–e48. [PubMed: 22184402]

9. Ter BP, Kristel P, van der Burg E, et al. Mechanisms of Therapy Resistance in Patient-Derived Xenograft Models of BRCA1-Deficient Breast Cancer. J Natl Cancer Inst. 2016;108: djw148.

10. Kemper K, Krijgsman O, Kong X, et al. BRAF(V600E) Kinase Domain Duplication Identified in Therapy-Refractory Melanoma Patient-Derived Xenografts. Cell Rep. 2016;16: 263–277. [PubMed: 27320919]

11. Bertotti A, Papp E, Jones S, et al. The genomic landscape of response to EGFR blockade in colorectal cancer. Nature. 2015;526: 263–267. [PubMed: 26416732]

12. Xue Z, Vis DJ, Bruna A, et al. MAP3K1 and MAP2K4 mutations are associated with sensitivity to MEK inhibitors in multiple cancer models. Cell Res. 2018;28: 719–729. [PubMed: 29795445]

13. Nicolle R, Blum Y, Marisa L, et al. Pancreatic Adenocarcinoma Therapeutic Targets Revealed by Tumor-Stroma Cross-Talk Analyses in Patient-Derived Xenografts. Cell Rep. 2017;21: 2458–2470. [PubMed: 29186684]

14. Braekeveldt N, von Stedingk K, Fransson S, et al. Patient-Derived Xenograft Models Reveal Intratumor Heterogeneity and Temporal Stability in Neuroblastoma. Cancer Res. 2018;78: 5958–5969. [PubMed: 30154149]

15. Prasetyanti PR, van Hooff SR, van Herwaarden T, et al. Capturing colorectal cancer inter-tumor heterogeneity in patient-derived xenograft (PDX) models. Int J Cancer. 2018;144: 366–371. [PubMed: 30151914]

16. Hao C, Wang L, Peng S, et al. Gene mutations in primary tumors and corresponding patient-derived xenografts derived from non-small cell lung cancer. Cancer Lett. 2015;357: 179–185. [PubMed: 25444907]

17. Perez-Soler R, Kemp B, Wu QP, et al. Response and determinants of sensitivity to paclitaxel in human non-small cell lung cancer tumors heterotransplanted in nude mice. Clin Cancer Res. 2000;6: 4932–4938. [PubMed: 11156254]

18. Zhang XC, Zhang J, Li M, et al. Establishment of patient-derived non-small cell lung cancer xenograft models with genetic aberrations within EGFR, KRAS and FGFR1: useful tools for preclinical studies of targeted therapies. J Transl Med. 2013;11: 168. [PubMed: 23842453]

19. Stewart EL, Mascaux C, Pham NA, et al. Clinical Utility of Patient-Derived Xenografts to Determine Biomarkers of Prognosis and Map Resistance Pathways in EGFR-Mutant Lung Adenocarcinoma. J Clin Oncol. 2015;33: 2472–2480. [PubMed: 26124487]

20. Kang HN, Choi JW, Shim HS, et al. Establishment of a platform of non-small-cell lung cancer patient-derived xenografts with clinical and genomic annotation. Lung Cancer. 2018;124: 168–178. [PubMed: 30268457]

21. Fichtner I, Rolff J, Soong R, et al. Establishment of patient-derived non-small cell lung cancer xenografts as models for the identification of predictive biomarkers. Clin Cancer Res. 2008;14: 6456–6468. [PubMed: 18927285]

22. Lee HW, Lee JI, Lee SJ, et al. Patient-derived xenografts from non-small cell lung cancer brain metastases are valuable translational platforms for the development of personalized targeted therapy. Clin Cancer Res. 2015;21: 1172–1182. [PubMed: 25549722]
23. Brown KM, Xue A, Mittal A, Samra JS, Smith R, Hugh TJ. Patient-derived xenograft models of colorectal cancer in pre-clinical research: a systematic review. Oncotarget. 2016;7: 66212–66225. [PubMed: 27517155]
24. Krepler C, Sproesser K, Brafford P, et al. A Comprehensive Patient-Derived Xenograft Collection Representing the Heterogeneity of Melanoma. Cell Rep. 2017;21: 1953–1967. [PubMed: 29141225]
25. Lissanu Deribe Y, Sun Y, Terranova C, et al. Mutations in the SWI/SNF complex induce a targetable dependence on oxidative phosphorylation in lung cancer. Nat Med. 2018;24: 1047–1057. [PubMed: 29892061]
26. Lee PC, Fang YF, Yamaguchi H, et al. Targeting PKCdelta as a Therapeutic Strategy against Heterogeneous Mechanisms of EGFR Inhibitor Resistance in EGFR-Mutant Lung Cancer. Cancer Cell. 2018;34: 954–969.e954.
27. Yan X, Zhang X, Wang L, et al. Inhibition of thioredoxin/thioredoxin reductase induces synthetic lethality in lung cancers with compromised glutathione homeostasis. Cancer Res. 2019;79: 125–132. [PubMed: 30401714]
28. Pu X, Zhang R, Wang L, et al. Patient-derived tumor immune microenvironments in patient-derived xenografts of lung cancer. J Transl Med. 2018;16: 328. [PubMed: 30477533]
29. John T, Yanagawa N, Kohler D, et al. Characterization of lymphomas developing in immunodeficient mice implanted with primary human non-small cell lung cancer. J Thorac Oncol. 2012;7: 1101–1108. [PubMed: 22617243]
30. Radaelli E, Hermans E, Omodho L, et al. Spontaneous Post-Transplant Disorders in NOD.Cg-Prkdcscid Il2rgtm1Sug/JicTac (NOG) Mice Engrafted with Patient-Derived Metastatic Melanomas. PLoS One. 2015;10: e0124974.
31. Dieter SM, Giessler KM, Kriegsmann M, et al. Patient-derived xenografts of gastrointestinal cancers are susceptible to rapid and delayed B-lymphoproliferation. Int J Cancer. 2017;140: 1356–1363. [PubMed: 27935045]
32. Bondarenko G, Ugolkov A, Rohan S, et al. Patient-Derived Tumor Xenografts Are Susceptible to Formation of Human Lymphocytic Tumors. Neoplasia. 2015;17: 735–741. [PubMed: 26476081]
33. Ilie M, Nunes M, Blot L, et al. Setting up a wide panel of patient-derived tumor xenografts of non-small cell lung cancer by improving the preanalytical steps. Cancer Med. 2015;4: 201–211. [PubMed: 25470237]
34. Guerrera F, Tabbo F, Bessone L, et al. The Influence of Tissue Ischemia Time on RNA Integrity and Patient-Derived Xenografts (PDX) Engraftment Rate in a Non-Small Cell Lung Cancer (NSCLC) Biobank. PLoS One. 2016;11: e0145100.
35. Butler KA, Hou X, Becker MA, et al. Prevention of Human Lymphoproliferative Tumor Formation in Ovarian Cancer Patient-Derived Xenografts. Neoplasia. 2017;19: 628–636. [PubMed: 28658648]
36. Economou JS, Belldegrun AS, Glaspy J, et al. In vivo trafficking of adoptively transferred interleukin-2 expanded tumor-infiltrating lymphocytes and peripheral blood lymphocytes. Results of a double gene marking trial. J Clin Invest. 1996;97: 515–521. [PubMed: 8567975]
37. Alexander RB, Rosenberg SA. Adoptively transferred tumor-infiltrating lymphocytes can cure established metastatic tumor in mice and persist long-term in vivo as functional memory T lymphocytes. J Immunother. 1991;10: 389–397. [PubMed: 1768672]
38. Williams SS, Chen FA, Kida H, et al. Engraftment of human tumor-infiltrating lymphocytes and the production of anti-tumor antibodies in SCID mice. J Immunol. 1996;156: 1908–1915. [PubMed: 8596043]
39. Simpson-Abelson MR, Sonnenberg GF, Takita H, et al. Long-term engraftment and expansion of tumor-derived memory T cells following the implantation of non-disrupted pieces of human lung tumor into NOD-scid IL2Rgamma(null) mice. J Immunol. 2008;180: 7009–7018. [PubMed: 18453623]

40. Wouters MCA, Nelson BH. Prognostic Significance of Tumor-Infiltrating B Cells and Plasma Cells in Human Cancer. Clin Cancer Res. 2018;24: 6125–6135. [PubMed: 30049748]

41. Gentles AJ, Newman AM, Liu CL, et al. The prognostic landscape of genes and infiltrating immune cells across human cancers. Nat Med. 2015;21: 938–945. [PubMed: 26193342]

42. Hernandez-Prieto S, Romera A, Ferrer M, et al. A 50-gene signature is a novel scoring system for tumor-infiltrating immune cells with strong correlation with clinical outcome of stage I/II non-small cell lung cancer. Clin Transl Oncol. 2015;17: 330–338. [PubMed: 25301404]

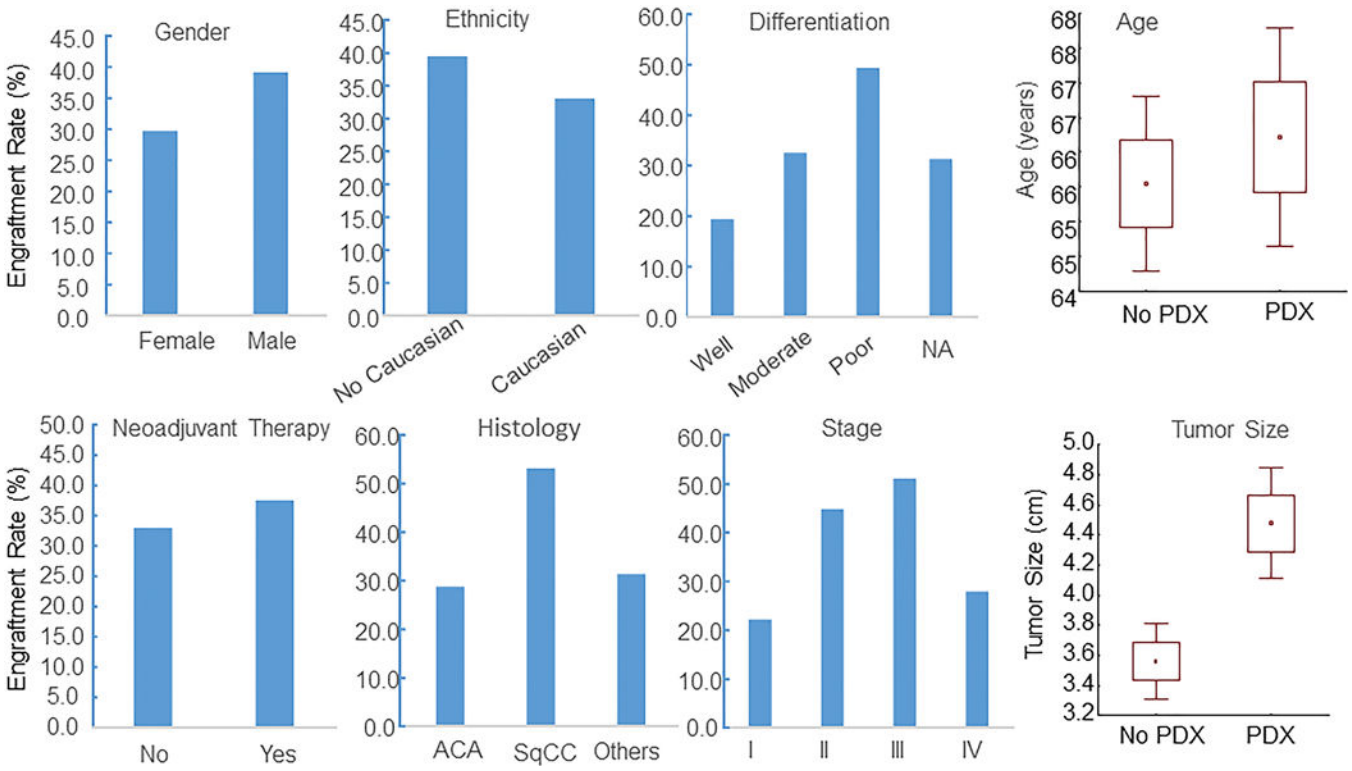

Figure 1.

Demographic and clinical parameters associated with engraftment of NSCLC PDXs. The parameters are shown at the top of each graph. The box plots for age and tumor size show the mean (small square) ± 1 SD (box) and ± SD (error bar). Tumor size differed significantly between implanted tumors with and without PDX growth ($P < 0.001$). ACA: adenocarcinoma; SqCC: squamous cell carcinoma.

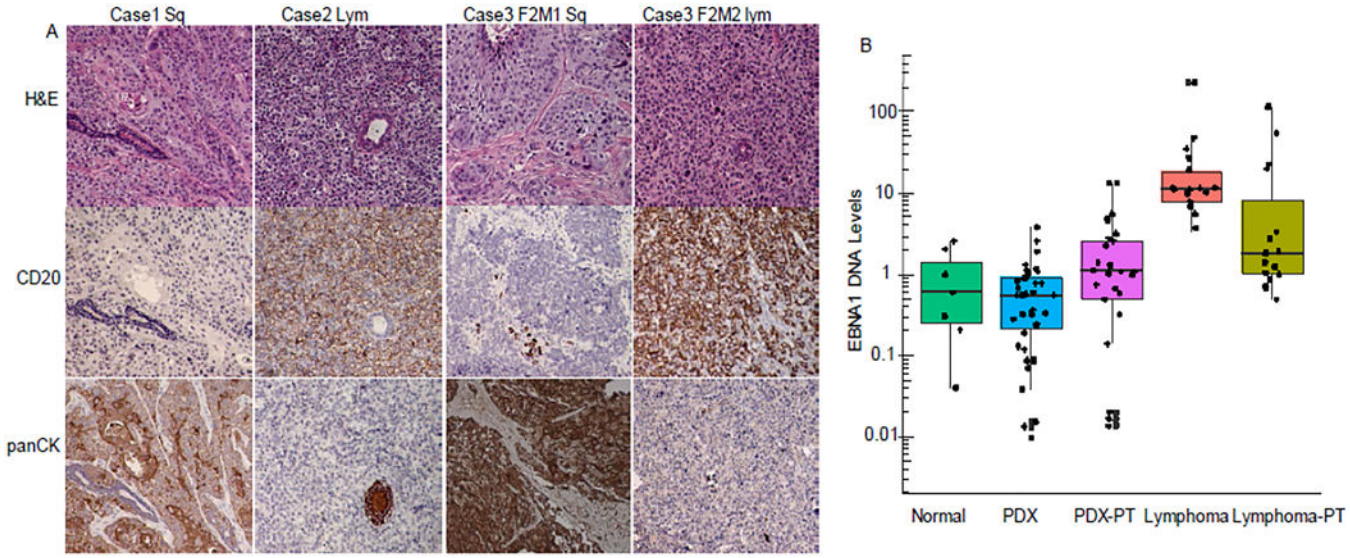

Figure 2.

Lymphoma formation during the process of generating PDXs. (A) Histological examples of NSCLC PDX and lymphoma. Anti-human CD20 and pan-cytokeratin (panCK) antibodies were used for immunohistochemical staining of human B cells and epithelial cells. Case 1 is an example of squamous cell carcinoma; Case 2, lymphoma. In Case 3, a passage 2 (F2) tumor was squamous cell carcinoma in mouse 1 (M1) but lymphoma in another mouse (M2). (B) *EBNA1* copy number in DNA samples as determined by qPCR. The copy number was normalized to that of the human *PERK* gene. The box plots show the mean (line inside box) ± 1SD (box) and ± SD (error bar), while the dots show individual values. Normal: peripheral blood mononuclear cells (PBMCs) from healthy donors (n = 7); PDX: PDX samples (n = 39); PDX-PT: primary tumors with successful PDX growth (n = 39); Lymphoma: lymphoma samples (n = 17); Lymphoma-PT (n = 15): primary tumors that resulted in lymphoma. The lymphoma significantly differed from the other groups ($P < 0.01$).

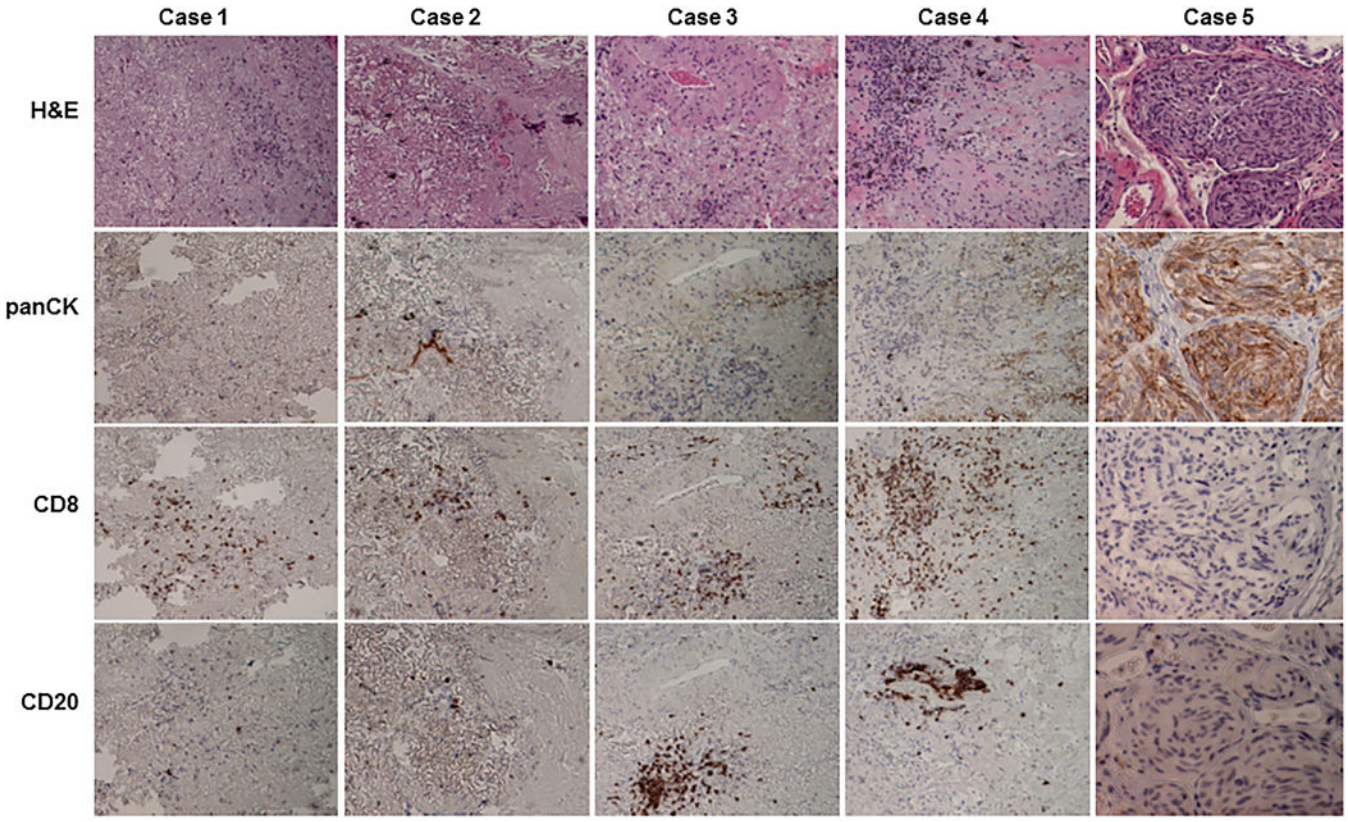

Figure 3.

Histological characterization of residual tumor tissue that did not form PDXs. Residual tumor tissues were harvested at 12 months after implantation from mice that showed no signs of PDX growth. On hematoxylin and eosin staining, the residual tumors from cases 1 to 4 were composed mainly of fibrotic tissues with scattered or clustered inflammatory cells. Case 5 had viable tumor cells. Immunohistochemical staining showed that inflammatory cells were human CD8+ or CD20+ cells, whereas cancer cells were positively stained for pan-cytokeratin (panCK).

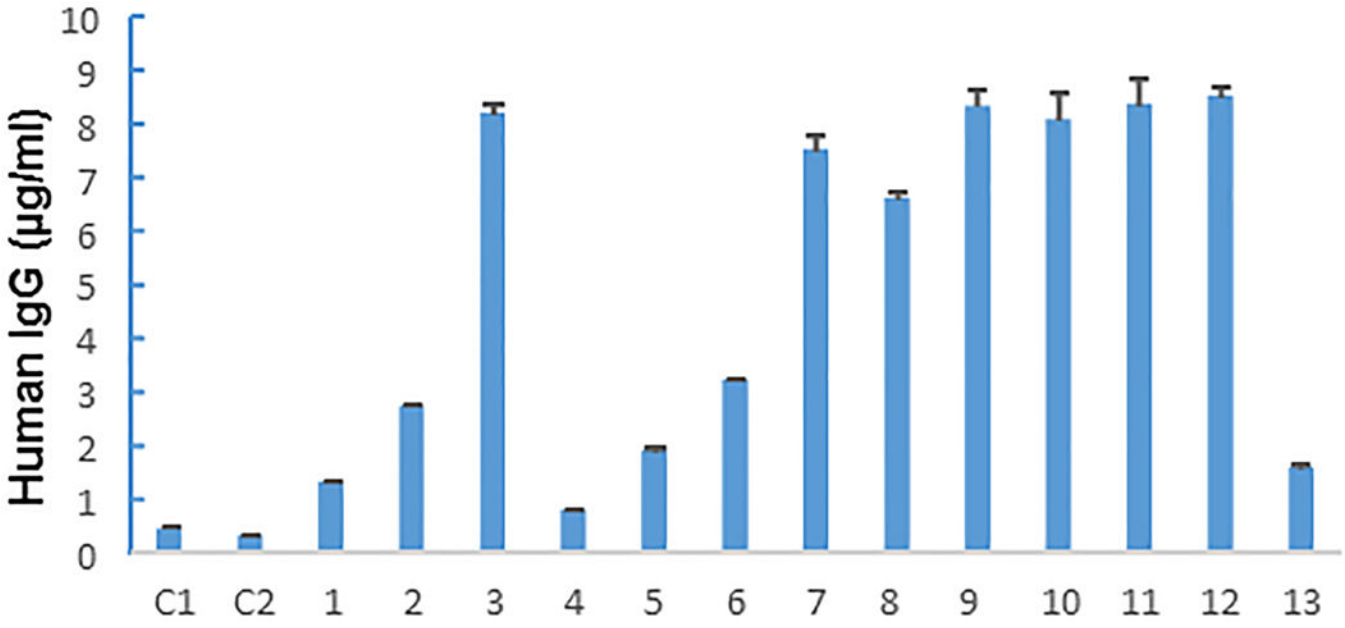

Figure 4.

Human immunoglobulin G (IgG) levels in mouse plasma samples. Plasma was collected from 2 control NSG mice (C1, C2) that never received human tissue implants and 13 NSG mice that did not have PDX growth at 14 months after implantation of primary tumor samples. Concentrations of human IgG were determined in triplicate for each sample. The values shown represent the mean ± SD of a triplicate assay. Twelve of the 13 mice that received implants but did not grow PDXs had >1 µg/mL human IgG in their plasma.

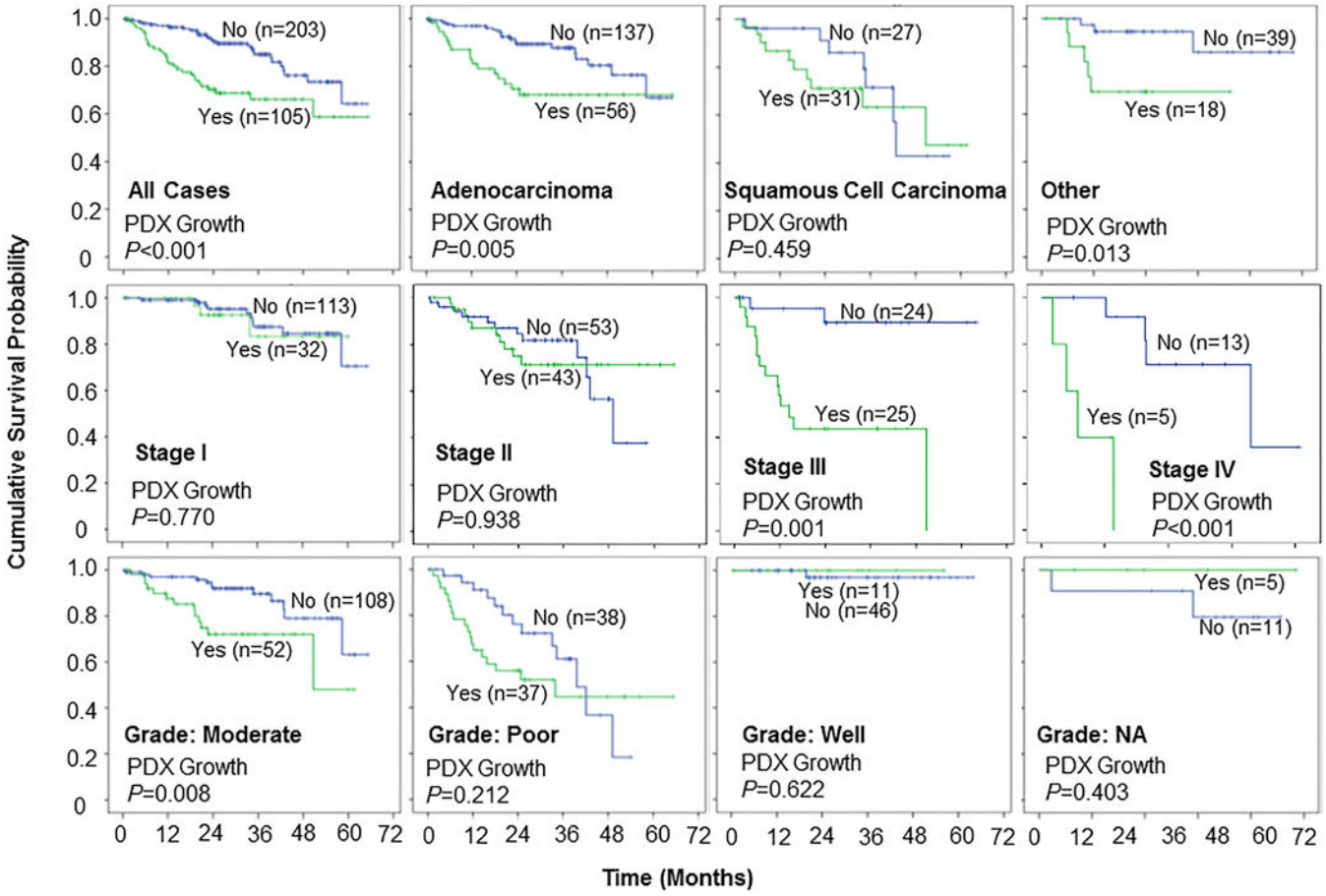

Figure 5.

Kaplan-Meier curves comparing overall survival by PDX growth status. Overall survival was significantly longer for patients whose tumors did not form PDXs in subsets of patients based on histology, disease stage, and degree of differentiation. Sample size (n) for the group with PDX growth (Yes, green line) or without PDX growth (No, blue line) was indicated in each panel.